Supporting Information for

Near-Infrared *C*-term MCD Spectroscopy of Octahedral Uranium(V) Complexes

Daniel J. Curran,[a†] Gaurab Ganguly,[b†] Yonaton N. Heit,[b] Nikki J. Wolford,[a] Stefan G. Minasian,[c] Matthias W. Löble,[d] Samantha K. Cary,[d] Stosh A. Kozimor,[d] Jochen Autschbach[b]* and Michael L. Neidig[a]*

[a]Department of Chemistry, University of Rochester, Rochester, New York 14627, USA

[b]Department of Chemistry, University at Buffalo, State University of New York, Buffalo, New York 14260, USA

[c]Chemical Sciences Division, Lawrence Berkeley National Laboratory, Berkeley, CA 94720

[d]Chemistry Division, Los Alamos National Laboratory, Los Alamos, New Mexico, 87544

Content

1. Experimental

1.1 Synthesis. All reagents not outlined herein were purchased from commercial sources. All air- and moisture-sensitive manipulations were carried out in an MBraun inert-atmosphere (N_2) glovebox equipped with a direct liquid nitrogen feed through the inlet line. All anhydrous solvents were freshly dried using activated alumina/4 Å molecular sieves and stored under an inert atmosphere. Synthesis of all complexes was prepared as previously reported.[1-5]

Preparation of UCl_4. An oven-dried three-neck 250 mL round bottom flask was fitted with a thermometer, a reflux condenser, and a glass stopper. 100 mL of hexachloropropene was added to the flask and purged with nitrogen for 15 minutes. The solution was heated to 190 °C and this temperature maintained throughout the reaction. About 5.5 g of UO_3 was placed in a scintillation vial. About 200 mg of the UO_3 was then added to the reaction under N_2 purge through the neck where the glass stopper was and allowed to stir for 30 minutes resulting in color changes from yellow to orange to dark red. After the 30 minutes of stirring, small amounts of UO_3 were added approximately every 5 minutes until all of UO3 was added. The reaction was allowed to stir for 14 hours at 190 °C. The UCl_4 formed as a green ppt at the bottom of the red solution. The reaction was placed under vacuum, pumped into the glovebox, and filtered through a medium pore frit. The solid was then washed with 20 mL toluene followed by two washes with 20 mL dichloromethane. The solid was dried under vacuum and stored in an N_2 glove box.

1.2 MCD Spectroscopy. All samples for MCD were prepared in an inert-atmosphere glovebox equipped with a liquid nitrogen fill port to allow for sample freezing at 77 K in the glovebox. Solid-state mulls of the complexes were prepared using ground polycrystalline samples and fluorolube as the mulling agent. NIR MCD experiments were conducted using a Jasco J-730 spectropolarimeter and liquid nitrogen-cooled InSb detector. The spectral range accessible with this NIR MCD setup is 2000–600 nm. UV-visible (UV-vis) MCD spectra were collected using a Jasco J-715 spectropolarimeter and a shielded S-20 photomultiplier tube. Both instruments utilize a modified sample compartment incorporating focusing optics and an Oxford Instruments SM4000-7T superconducting magnet/cryostat, permitting measurements from 1.6 K to 290 K with magnetic fields up to 7 T. All MCD spectra were baseline-corrected against zero-field scans. All spectra are averaged over 4 scans with data being collected at a rate of 100 nm/min.

2. Computational Details

2.1 Kohn-Sham Theory

Structures of the $[UX_6]^-$ (X = F, Cl) complexes in the O_h point group symmetry were optimized with the B3LYP hybrid functional,[6] 60-electron scalar relativistic effective core potential (ECP)[7] and a corresponding Gaussian-type ECP60MWB_SEG valence basis[8] for U, and the 6-311+G(d) basis for the halogens, using Gaussian 16.[9] Harmonic vibrational modes and frequencies were calculated analytically at the same level at which geometry optimizations were performed. The seven nuclei of each complex give rise to 15 internal degrees of freedom, and they can be grouped into six by symmetry: $\nu_1(a_{1g})$, $\nu_2(e_g)$, $\nu_3(t_{2g})$, $\nu_4(t_{1u})$, $\nu_5(t_{1u})$, and $\nu_6(t_{2u})$.[10] Vibrations along the ungerade modes, $\nu_4(t_{1u})$, $\nu_5(t_{1u})$, and $\nu_6(t_{2u})$, can generate vibronic intensities for 5f-to-5f LF transitions,[10,11] through the coupling of opposite parity states, leading to the "intensity borrowing". The vibrational frequencies of the ungerade modes are compared to the experimental values in Table S1. The calculated frequencies were in excellent agreement with the experimental data, allowing simulations of the LF MCD spectra using those frequencies. As mentioned before, experimental structures were used for H-T expansion, and therefore, the vibrational normal modes obtained from the optimized O_h structures were subsequently mapped onto the slightly distorted experimental structures for the vibronic calculations. Given the approximations that had to be made to render the computations tractable, in particular the use of the same vibrational modes for the different electronic states, the use of a slightly distorted structure on which the HT expansion is carried out provides at lease some accommodation of the minor symmetry lowering in the solids.

Table 1: Calculated Gas-Phase Vibrational Frequencies (cm^{-1}) for the Ungerade Symmetry Inducing Normal Modes Responsible for Vibronic Coupling.[a]

	$[UF_6]^-$		$[UCl_6]^-$	
	Calc.	Expt.[b]	Calc.	Expt.[b]
ν_4 (t_{1u})	173	170	114	119
ν_5 (t_{1u})	516	525	300	308
ν_6 (t_{2u})	133	129	82	94

[a]Vibrational frequencies were calculated analytically with B3LYP/ECP60MWB/6-3111+G(d) for $[UX_6]^-$ (X = F, Cl)
[b]Experimental vibrational frequencies for $(C_6H_5)_4AsUF_6$ and $(C_2H_5)_4NUCl_6$ are taken from ref. 31.

2.2 Wave Theory Calculations

Ab initio wavefunction calculations were performed using the Restricted Active Space (RAS) self-consistent field (SCF) method,[12,13] a variant of the complete active space (CAS) SCF method,[14] using a current developers' version of the OpenMolcas software.[15] In RAS calculations, the active space is partitioned into three sub-spaces RAS1/2/3, and electronic configurations are generated by a pre-selected maximum number of holes/particles in RAS1/3, while RAS2 remains unrestricted. Scalar relativistic (SR) effects in the wavefunction calculations were considered via the all-electron second-order Douglas-Kroll-Hess (DKH2) Hamiltonian[16,17] in combination with relativistically contracted all-electron triple-ζ quality ANO-RCC-VTZP basis sets.[18,19] Spin-orbit (SO) coupling was treated via RAS state-interaction (RASSI) of the SR RAS wavefunctions, using atomic mean-field SO integrals (AMFI).[20] In this article, RAS-SO and PT2-SO designations are used to indicate whether the diagonal elements of the SO Hamiltonian were 'dressed' with RAS or multi-state PT2 energies. Here, PT2 refers to a treatment of the dynamic electron correlation in the SR calculations by second-order perturbation theory. The non-abelian O_h point group is not supported in Molcas. Instead, the calculations were performed using the C_i abelian subgroup, preserving the inversion symmetry of the complexes so that U 5f, U 6d, and ligand-centered basis orbitals span different parity.

In $[UX_6]^-$ (X = F, Cl), the 7-fold degenerate U 5f shell splits into a_{2u}, t_{2u}, and t_{1u} species in the O_h LF.[10, 11] The 6d shell split into t_{2g} and e_g species. The valence p AOs of the six halides form 18 symmetry-adapted ligand group orbitals (LGOs), six of them are σ-interacting (a_{1g}, e_g, and t_{1u}) and the rest are π-interacting (t_{1g}, t_{2g}, t_{1u}, and t_{2u}) with the U center.[10] The linear combinations of metal-centered AOs with matching symmetry LGOs form the valence MOs, where U 5f orbitals remain mostly non-bonding. The RAS partitioning follows Ref 10 to account for a sufficient number of dipole-allowed LMCT and 5f-to-6d to "borrow" the intensity of dipole-forbidden 5f-to-5f LF transitions through the vibronic coupling.

The 9 g symmetry LGOs (a_{1g}, e_g, t_{1g}, t_{2g}) with 18 electrons and 1 hole allowed constituted RAS1. RAS2 consisted of the seven U 5f orbitals (a_{2u}, t_{1u}, and t_{2u}). Moreover, five 6d orbitals (t_{2g} and e_g) with at most 1 electron constituted RAS3 to model the 5f-to-6d transitions. This active space partitioning, denoted as RAS(18,9|1,7|0,5), accounts for a sufficient number of dipole-allowed LMCT and 5f-to-6d transitions to facilitate the vibronic intensity of dipole-forbidden LF transitions. The u and g symmetry states were targeted separately, in the C_i point group. The chosen RAS partitioning generates the following number of spin-free (SF) states: 7 spin-doublets in A_u symmetry corresponding to 5f-to-5f LF transitions, 441 spin-doublets, and 189 spin-quartets in Ag symmetry (depending upon spin-pairing) corresponding to LMCT transitions, and 5 spin-doublets in A_g symmetry corresponding to 5f-to-6d transitions. However, due to the large computational cost of the PT2 calculation, the number of LMCT states was truncated at 131 spin-doublets and 54 spin-quartets in A_g symmetry.

2.3 Choice of Structures: Simulated NIR *C*-term MCD Spectra of $[UCl_6]^-$ and $[UF_6]^-$

For describing the orbitals, vibrational modes, and properties of $[UX_6]^-$ (X = F, Cl) complexes, O_h point group symmetry has been used in the literature.[10,11,21-29] However, crystallographic structures show to have slight deviations from O_h point group symmetry (e.g. D_{4h}, D_{3d}, and C_i) depending upon the complex's counter cation.[1,28-32] In the following, we infer that the MCD spectra in the NIR region are likely to be very sensitive to the geometric perturbations and the deviations from O_h point group symmetry. Experimental structures were used for H-T expansion, and therefore, the vibrational normal modes obtained from the optimized O_h structures were subsequently mapped onto the slightly distorted experimental structures for the vibronic calculations. These assumptions provide insight into the U(V) ion's ability to accommodate for small distortions.

3. Supplemental Figures with Experimental and Calculated MCD Spectra

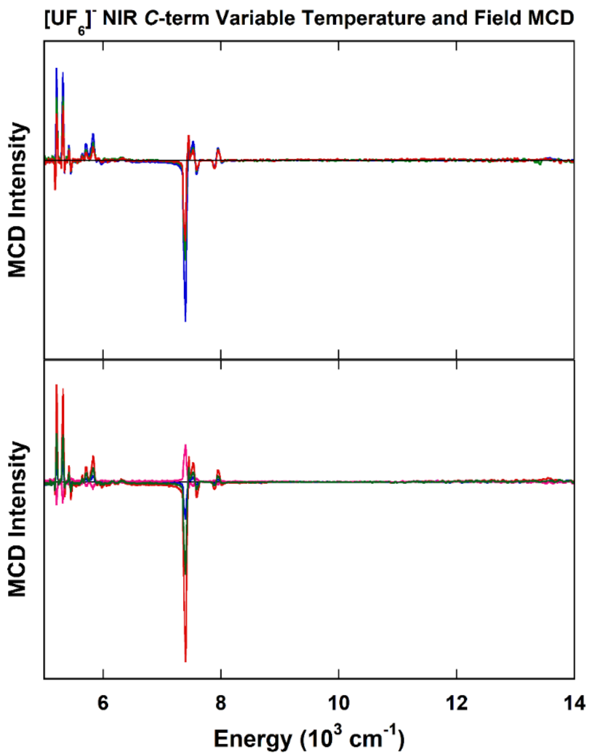

Fig. S1. Variable Temperature and Field $\boldsymbol{C}$-term MCD spectra of $[UF_6]^-$ Complexes To demonstrate the $\boldsymbol{C}$-term nature of the transitions, variable temperature, and field scans were taken for $[UF_6]^-$. (Top) The 7 T, variable temperature spectra were recorded at 5 K (blue), 10 K (green), and 15 K (red). Note that the baseline was run at 0 T. (Bottom) The 5 K, variable field spectra recorded at 7 T (red), 3.5 T, (green) 1.5 T (blue), 0 T (black), and -3.5 T (pink).

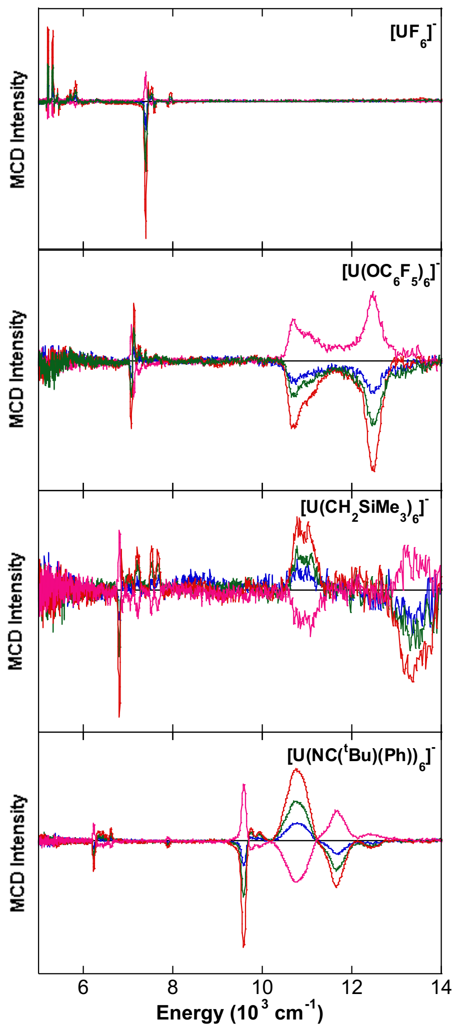

Fig. S2. 5 K, Variable Field NIR ***C***-term MCD spectra of U(V) O_h Complexes.
The fields utilized were 7 T (red), 3.5 T, (green) 1.5 T (blue), 0 T (black), and -3.5 T (pink).

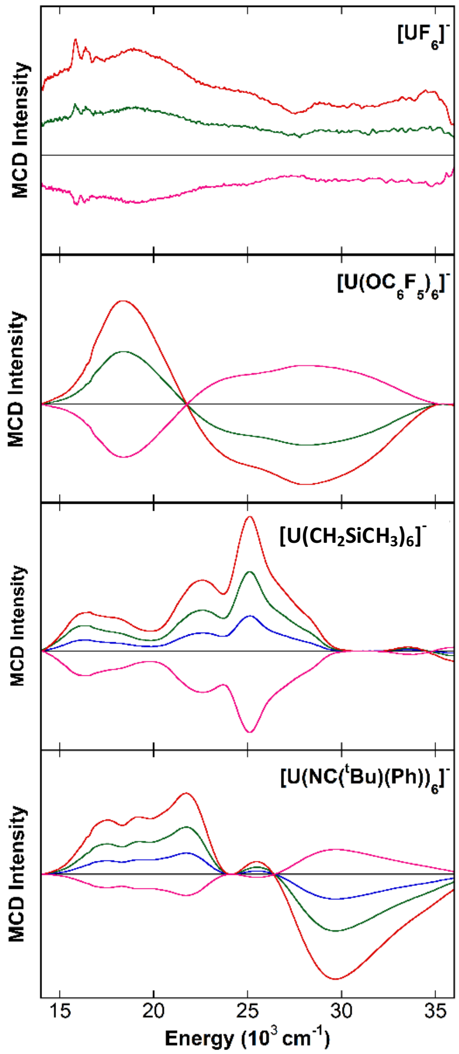

Fig. S3. 5 K, Variable Field UV-Vis ***C***-term MCD spectra of different U(V) O_h Complexes. The fields utilized were 7 T (red), 3.5 T, (green) 1.5 T (blue), 0 T (black), and -3.5 T (pink). The variable field UV-Vis ***C***-term MCD spectra of $[UCl_6]^-$ has been previously reported.[1]

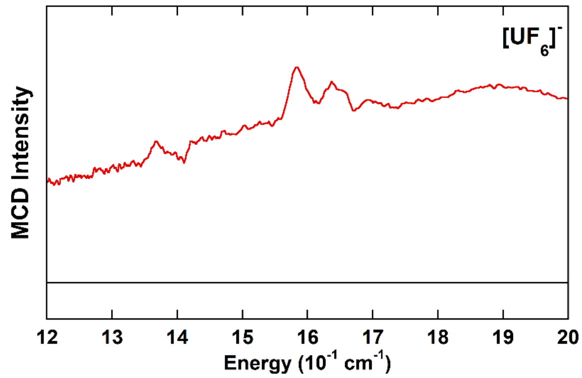

Fig S4. 5 K, 7 T UV-Vis ***C***-term MCD spectrum of $[UF_6]^-$ of highlighting the $\Gamma_7 \rightarrow \Gamma_{8'}$ and $\Gamma_7 \rightarrow \Gamma_6$ transitions.

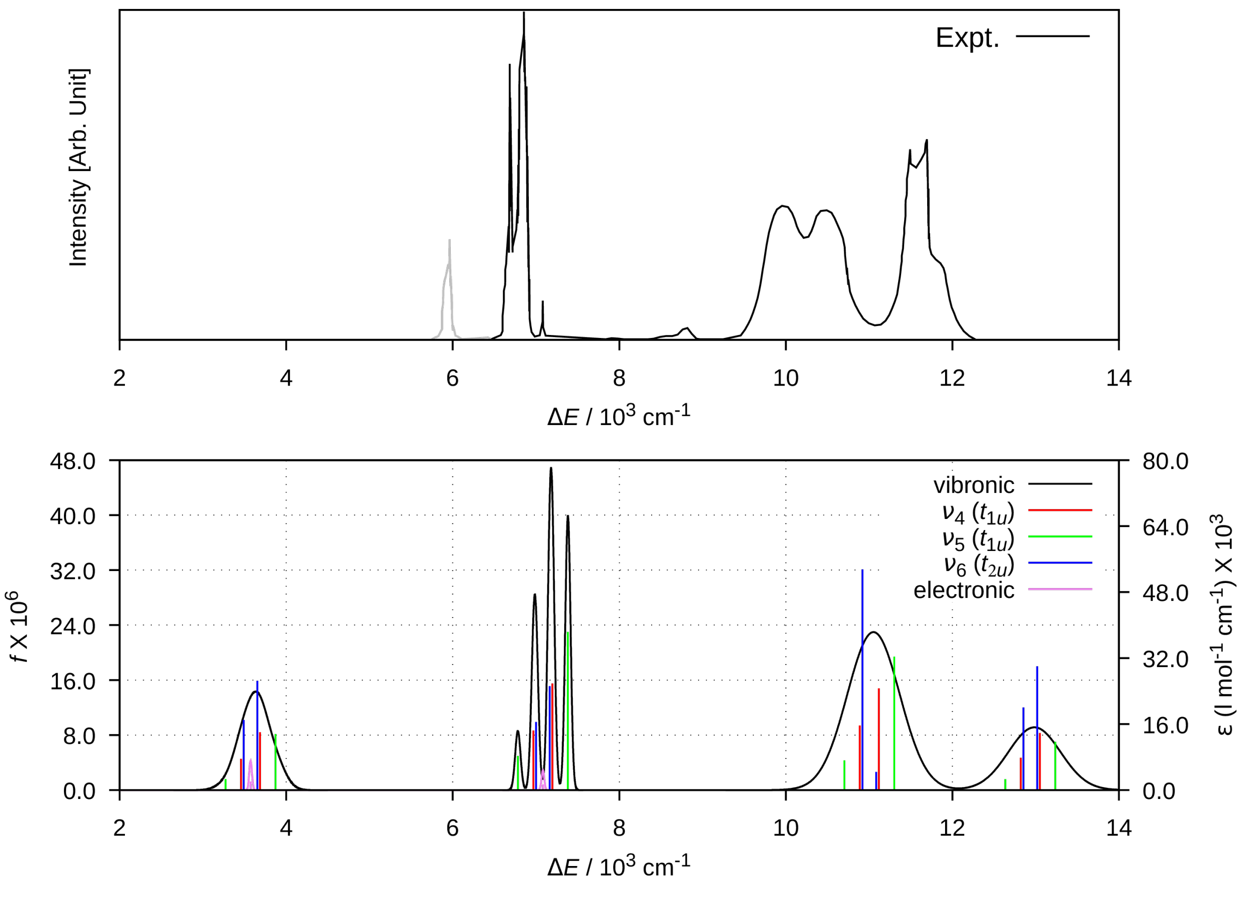

Fig. S5. 5f-to-5f LF spectrum of $[UCl_6]^-$. Top: the experimental LF spectrum [for solid $(C_6H_5)_4AsUCl6$] was digitized from Figure 4 in ref S1. Bottom: the LF spectrum calculated with PT2-SO. The left-vertical axis represents the oscillator strength (f), and the right-vertical axis represents the extinction coefficient ε. The calculated spectra were Gaussian-broadened, with $\sigma = 120$ cm^{-1} for vibronic $E_{5/2u} \rightarrow F_{3/2u}$ transitions, $\sigma = 32$ cm^{-1} for $E_{5/2u} \rightarrow E_{5/2u}{}'$, and $\sigma = 280$ cm^{-1} elsewhere, to qualitatively reproduce the relative experimental band peak heights. Electronic magnetic dipole transitions were broadened with a Gaussian broadening of $\sigma = 16$ cm^{-1} to match the appearance of the magnetic $E_{5/2u} \rightarrow E_{5/2u}{}'$ peak in the experiment. The contributions of different inducing modes are denoted with different colors in the underlying "stick spectra".

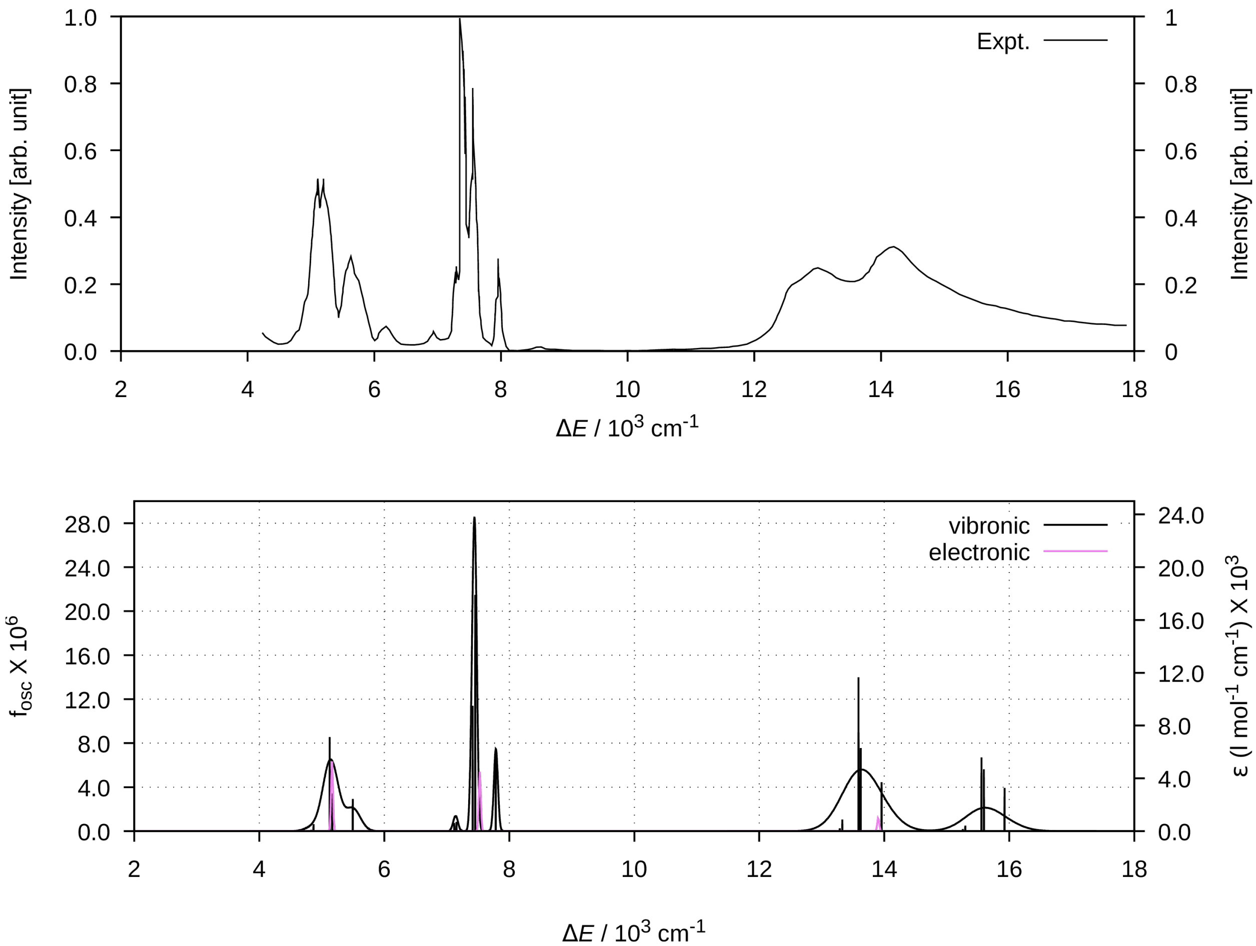

Fig. S6. 5f-to-5f LF spectrum of $[UF_6]^-$. Top: the experimental LF spectrum [for solid $CsUF_6$] was digitized from Figure 4 in ref S2. Bottom: the LF spectrum calculated with PT2-SO. The left-vertical axis represents the oscillator strength (f), and the right-vertical axis represents the extinction coefficient ε. The calculated spectra were Gaussian-broadened, with $\sigma = 120\ cm^{-1}$ for vibronic $E_{5/2u} \rightarrow F_{3/2u}$ transitions, $\sigma = 32\ cm^{-1}$ for $E_{5/2u} \rightarrow E_{5/2u}'$, and $\sigma = 280\ cm^{-1}$ elsewhere, to qualitatively reproduce the relative experimental band peak heights. Electronic magnetic dipole transitions were broadened with a Gaussian broadening of $\sigma = 16\ cm^{-1}$ to match the appearance of the magnetic $E_{5/2u} \rightarrow E_{5/2u}'$ peak in the experiment.

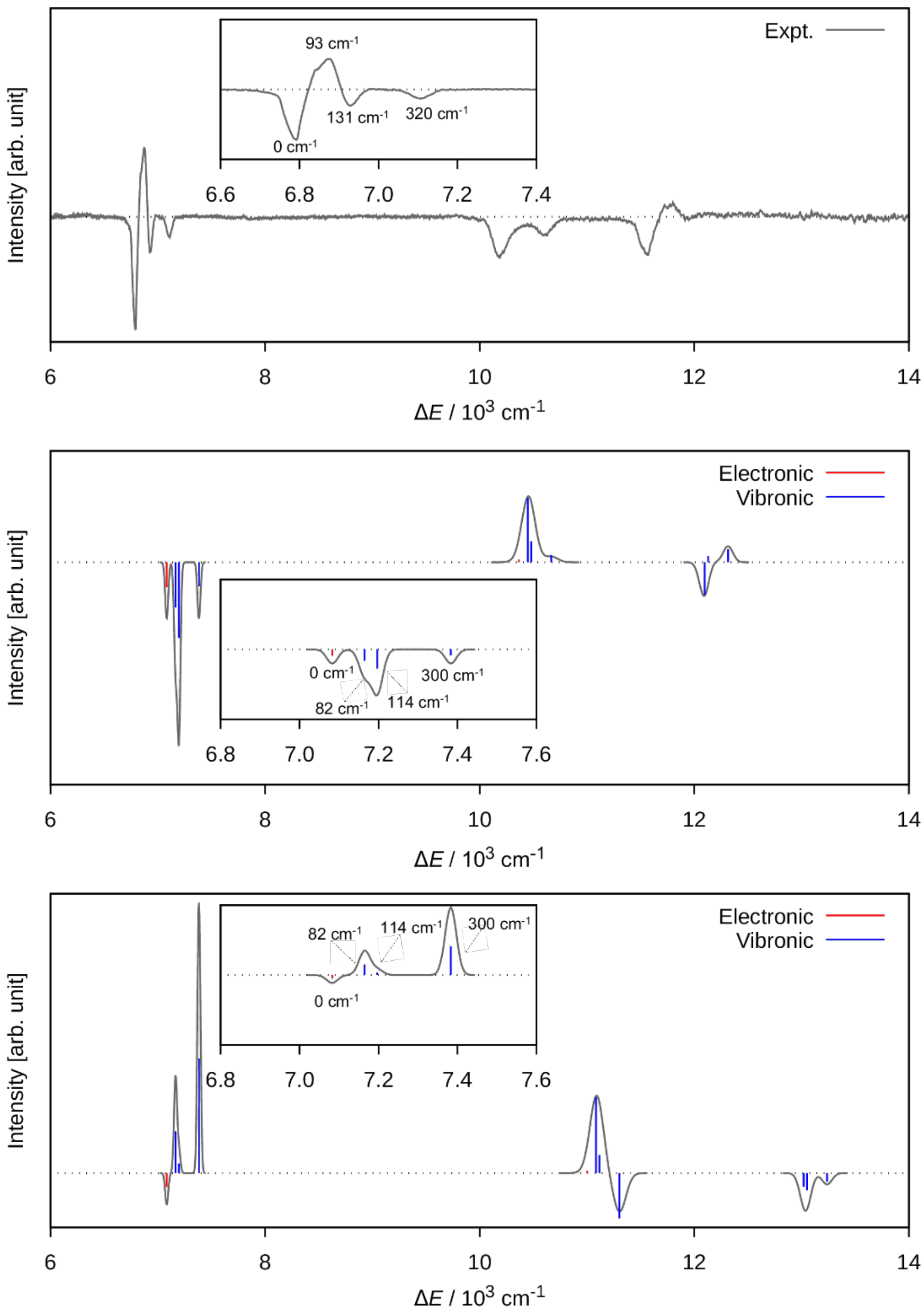

Fig. S7. 5f-to-5f LF MCD spectra of $[UCl_6]^-$: Top: the experimental LF spectrum. Middle: LF MCD spectra (5 K) calculated with RAS-SO using O_h structure for H-T expansion. Bottom: LF MCD spectra (5 K) calculated with PT2-SO using O_h structure for H-T expansion. Calculated $\Gamma_7 \rightarrow \Gamma_{7'}$ transitions were Gaussian-broadened with FWHM = 25 cm-1, $\Gamma_7 \rightarrow \Gamma_8$ transitions were Gaussian-broadened with FWHM = 200 cm^{-1}, and $\Gamma_7 \rightarrow \Gamma_6$ transitions were Gaussian-broadened with FWHM = 150 cm^{-1}. The sharp and intense $\Gamma_7 \rightarrow \Gamma_{7'}$ LF MCD peaks are shown in the inset for clarity. The contributions of electronic and vibronic transitions are denoted with different colors in the underlying "stick spectra".

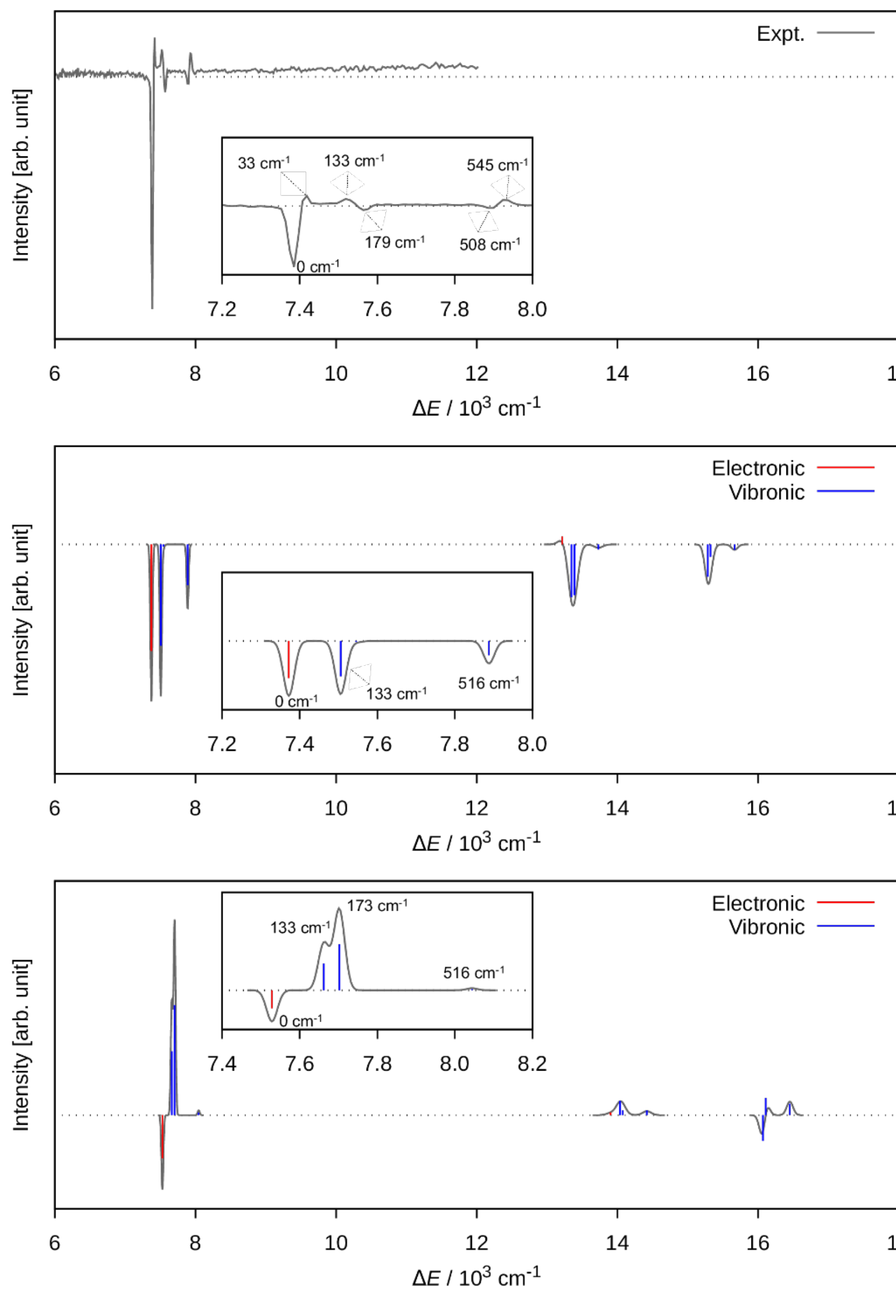

Fig. S8. 5f-to-5f LF MCD spectra of $[UF_6]^-$: Top: the experimental LF spectrum. Middle: LF MCD spectra (5 K) calculated with RAS-SO using O_h structure for H-T expansion. Bottom: LF MCD spectra (5 K) calculated with PT2-SO using O_h structure for H-T expansion. Calculated $\Gamma_7 \rightarrow \Gamma_{7'}$ transitions were Gaussian-broadened with FWHM = 25 cm^{-1}, $\Gamma_7 \rightarrow \Gamma_8$ transitions were Gaussian-broadened with FWHM = 200 cm^{-1}, and $\Gamma_7 \rightarrow \Gamma_6$ transitions were Gaussian-broadened with FWHM = 150 cm^{-1}. The sharp and intense $\Gamma_7 \rightarrow \Gamma_{7'}$ LF MCD peaks are shown in the inset for clarity. The contributions of electronic and vibronic transitions are denoted with different colors in the underlying "stick spectra".

References

1. Gendron, F.; Fleischauer, V. E.; Duignan, T. J.; Scott, B. L.; Löble, M. W.; Cary, S. K.; Kozimor, S.; Bolvin, H.; Neidig, M. L.; Autschbach, *J. Phys. Chem. Chem. Phys.* 2017, **19**, 17300-17313
2. S. Fortier, G. Wu., and T. W. Hayton, *Inorg. Chem.*, 2009, **48**, 3000-3011
3. S. Fortier, J. R. Walensky, G. Wu, and T. W. Hayton, *J. Am. Chem. Soc.*, 2011, **133**, 11732-11743
4. L. A. Seaman, G. Wu, N. Edelstein, W. W. Lukens, N. Magnani, and T. W. Hayton, *J. Am. Chem. Soc.*, 2012, **134**, 4931-4940
5. C. G. Gianopoulos, V. V. Zhurov, S. G. Minasian, E. R. Batista, C. Jelsch and A. A. Pinkerton, *Inorg. Chem.*, 2017, **56**, 1775-1778.
6. Becke, A. D. *J. Chem. Phys.* 1993, **98**, 5648−5652
7. Cao, X.; Dolg, M.; Stoll, H. *J. Chem. Phys.* 2003, **118**, 487−496
8. Cao, X.; Dolg, M. *J. Mol. Struct.: THEOCHEM* 2004, **673**, 203−209.
9. Frisch, M. J.; Trucks, G. W.; Schlegel, H. B.; Scuseria, G. E.; Robb, M. A.; Cheeseman, J. R.; Scalmani, G.; Barone, V.; Petersson, G. A.; Nakatsuji, H. et al. Gaussian 16, revision C.01; Gaussian, Inc.: Wallingford, CT, 2016. www.gaussian.com
10. Ganguly, G.; Ludoweig, H. D.; Autschbach, J. *J. Chem. Theory Comput.* 2020, **16**, 5189–5202
11. Heit, Y. N.; Gendron, F.; Autschbach, J. *J. Phys. Chem. Lett.* 2018, **9**, 887–894
12. Malmqvist, P. Å.; Rendell, A.; Roos, B. O. *J. Phys. Chem.* 1990, **94**, 5477–5482.
13. Olsen, J.; Roos, B. O.; Jørgensen, P.; Jensen, H. J. A. *J. Chem. Phys.* 1988, **89**, 2185–2192.
14. Roos, B. O.; Taylor, P. R.; Siegbahn, P. E. *M. Chem. Phys.* 1980, **48**, 157-173.
15. Aquilante, F.; Autschbach, J.; Baiardi, A.; Battaglia, S.; Borin, V. A.; Chibotaru, L. F.; Conti, I.; De Vico, L.; Delcey, M.; Galván, I. F.; Ferré, N.; Freitag, L.; Garavelli, M.; Gong, X.; Knecht, S.; Larsson, E. D.; Lindh, R.; Lundberg, M.; Malmqvist, P. Å.; Nenov, A.; Norell, J.; Odelius, M.; Olivucci, M.; Pedersen, T. B.; Pedraza-González, L.; Phung, Q. M.; Pierloot, K.; Reiher, M.; Schapiro, I.; Segarra-Martí, J.; Segatta, F.; Seijo, L.; Sen, S.; Sergentu, D.-C.; Stein, C. J.; Ungur, L.; Vacher, M.; Valentini, A.; and Veryazov, V. *J. Chem. Phys*. 2020, **152**, 214117.
16. van Lenthe, E.; Baerends, E. J.; Snijders, J. G. *J. Chem. Phys.* 1993, **99**, 4597-4610.
17. Wolf, A.; Reiher, M.; Hess, B. A. *J. Chem. Phys.* 2002, **117**, 9215-9226.
18. Roos, B. O.; Lindh, R.; Malmqvist, P.-Å.; Veryazov, V.; Widmark, P.-O. *J. Phys. Chem. A* 2005, **109**, 6575.
19. Roos, B. O.; Lindh, R.; Malmqvist, P.-Å.; Veryazov, V.; Widmark, P.-O. *J. Phys. Chem. A* 2004, **108**, 2851–2858.
20. Malmqvist, P.-A.; Roos, B. O.; Schimmelpfennig, B. *Chem. Phys. Lett.* 2002, **357**, 230-240.
21. Minasian, S. G.; Keith, J. M.; Batista, E. R.; Boland, K. S.; Clark, D. L.; Conradson, S. D.; Kozimor, S. A.; Martin, R. L.; Schwarz, D. E.; Shuh, D. K.; Wagner, G. L.; Wilkerson, M. P.; Wolfsberg, L. E.; Yang, P. *J. Am. Chem. Soc*. 2012, **134**, 5586-5597.
22. Kaltsoyannis, N.; Bursten, B. E. Inorg. Chem. 1995, 34, 2735-2744.
23. Lukens, W. W.; Edelstein, N. M.; Magnani, N.; Hayton, T. W.; Fortier, S.; Seaman, L. A. *J. Am. Chem. Soc.* 2013, **135**, 10742-10754
24. Selbin, J.; Ortego, J. D.; Gritzner, G. *Inorg. Chem.* 1968, **7**, 976-982.
25. Edelstein, N.; Brown, D.; Whittaker, B. *Inorg. Chem.* 1974, **3**, 563-567.
26. Verma, P.; Autschbach, J. *J. Chem. Theory Comput.* 2013, **9**, 1052–1067.
27. Notter, F.-P.; Bolvin, H. *J. Chem. Phys.* 2009, **130**, 184310–11.
28. Eastman, M. P.; Eller, P. G.; Halstead, G. W. J. *Inorg. Nucl. Chem.* 1981, **43**, 2839–2842.
29. Gianopoulos, C. G.; Zhurov, V. V.; Minasian, S. G.; Batista, E. R.; Jelsch, C.; Pinkerton, A. A. *Inorg. Chem.* 2017, **56**, 1775–1778.
30. Hecht, H. G.; Malm, J. G.; Foropoulos, J.; Carnall, W. T. *J. Chem. Phys.* 1986, **84**, 3653– 3662.

31. Leung, A. F. *J. Phys. Chem. Solids* 1977, **38**, 529–532.
32. Rosenzweig, A.; Cromer, D. T. *Acta Cryst.* 1967, **23**, 865–867.